CrystEngComm

PAPER

View Article Online
View Journal | View Issue

Cite this: *CrystEngComm*, 2014, **16**, 3323

Selective synthesis of copper gallium sulfide ($CuGaS_2$) nanostructures of different sizes, crystal phases, and morphologies†

Shu-Hao Chang,‡ Bo-Cheng Chiu,‡ Tzu-Lun Gao, Shao-Lou Jheng and Hsing-Yu Tuan*

Received 11th December 2013,
Accepted 23rd January 2014

DOI: 10.1039/c3ce42530d

www.rsc.org/crystengcomm

$CuGaS_2$ nanostructures with different sizes, phases and morphologies were prepared. Chalcopyrite $CuGaS_2$ nanocrystals with sizes ranging from 3.0 to 10.9 nm were synthesized using $GaCl_3$, CuCl, and elemental sulfur as the precursors at temperatures ranging from 180 to 240 °C in hot-solvent synthesis. The $CuGaS_2$ nanocrystals show size-dependent optical absorption and photoluminescence properties, exhibiting a quantum confinement effect. Wurtzite $CuGaS_2$ nanostructures could be synthesized by replacing elemental sulfur with thiourea as the S source. We find that the amount of oleylamine (OLA) significantly affects the morphologies of the $CuGaS_2$ nanostructures: $CuGaS_2$ nanowires tend to form while the amount of OLA in the reaction decreased. The growth mechanism of $CuGaS_2$ nanowires is proposed based on the experimental observation of morphology evolution from 130 to 240 °C.

1. Introduction

I–III–VI_2 chalcopyrite semiconductor materials such as $CuInS_2$, $CuInSe_2$ and $CuInGaSe_2$ are receiving significant attention as thin film absorbing layers in photovoltaic devices due to their promising characteristics, including suitable direct energy gap energies to the solar spectrum, high absorption coefficient (10^5 cm^{-1}) with good electrical stability and good radiation stabilities.[1–3] Nano-sized I–III–VI_2 ternary compounds have been particularly influential in photovoltaics,[4–8] energy storage fields[9,10] and medical imaging applications.[11] The attractive point of these nanomaterials is that they can be directly implemented in advanced applications through the solution-based deposition process without high-vacuum equipment. This greatly reduces the fabrication cost[12–15] and is the future trend to photovoltaic manufacturing procedure for mass production.[16] In recent years, many synthetic techniques of I–III–VI_2 nanocrystals, such as solvothermal reactions,[17,18] hot-solvent synthesis,[19–23] and seed catalytic growth[24] have been intensively investigated. Synthetic methods coupled with a resolved mechanism are therefore of special importance.

The size, phase and shape of nanocrystals closely interact with the nanocrystal properties.[25] Some interesting works have been done in the field of nanomaterial synthesis. For example, Yarema *et al.* have controlled the size of $CuInSe_2$ nanocrystals between 2.7 and 7.9 nm by varying the reaction time and reaction temperature.[26] On the other hand, shape control has raised interest for the fabrication of semiconductor nanocrystals because of its correlation with physical properties or chemical reactivity. For instance, one-dimensional (1D) nanomaterials, (*e.g.* nanorods and nanowires) have been observed to exhibit different optical properties, such as emission polarization.[27] Although 1D nanostructures can be fabricated through a wide range of advanced nanolithography, including electron-beam and focused-ion-beam writing, in order to achieve low-cost, large-scale production, new synthetic techniques should be developed. For nanocrystal synthesis, three strategies are usually applied for the fabrication of 1D nanostructures in chemical synthesis: (i) template-assisted anisotropic growth; (ii) capping reagents-guided kinetic anisotropic growth,[28] and (iii) oriented attachment-mediated assembly of nanoparticles to nanowires.[29–33] Further, materials with different phases also exhibit distinct properties. For example, wurtzite phases of I–III–VI_2 materials exhibit different optical properties since they offer a higher flexibility of stoichiometry control due to random distribution of the I and III groups of ions, which may be advantageous for solar cell applications.[34,35]

$CuGaS_2$ nanocrystals have a direct bandgap of 2.49 eV with a high absorption coefficient (10^5–10^6 cm^{-1}).[36,37] However, the reactivity of the Ga precursor is different from that of other compositions, leading to free gallium nuclei in the reaction.[35] There have been some reports on the synthesis of

Department of Chemical Engineering, National Tsing Hua University, 101, Section 2, Kuang-Fu Road, Hsinchu, Taiwan 30013, Republic of China. E-mail: hytuan@che.nthu.edu.tw; Fax: +886 3 571 5408; Tel: +886 3 572 3661

† Electronic supplementary information (ESI) available: EDS data. See DOI: 10.1039/c3ce42530d

‡ These authors contributed equally.

$CuGaS_2$ nanocrystals through hydrothermal and solvothermal methods. However, most of nanoparticles appear in the form of large crystallites.[38,39] Very recently, the wurtzite phase of $CuGaS_2$ nanocrystals has been synthesized.[37,40] However, studies to systematically control the synthesis of $CuGaS_2$ nanomaterials are still lacking.

In this report, chalcopyrite $CuGaS_2$ nanocrystals with diameters ranging from 3.0 to 10.9 nm were obtained using $GaCl_3$, CuCl, and elemental sulfur as the precursors at temperatures ranging from 180 to 240 °C in hot-solvent synthesis. The size-dependent optical properties of $CuGaS_2$ nanocrystals are observed from the optical absorption and photoluminescence (PL) spectra, showing their quantum confinement effect. On the other hand, by changing the sulfur source from sulfur powder to thiourea, wurtzite $CuGaS_2$ nanocrystals were obtained. Further, by decreasing the amount of oleylamine (OLA) in the synthesis, wurtzite nanowires were formed. This study represents a systematic approach to selectively obtain $CuGaS_2$ nanostructures with different sizes, phases, and morphologies.

2. Experimental details

Materials

Copper(I) chloride (CuCl, 99.99%), gallium(III) chloride ($GaCl_3$, 99.99%), oleylamine (OLA, 97%) and sulfur powder (S, 99.99%), 1-dodecanethiol (DDT, 98%), thiourea, dodecylamine (DDA) and ethanol (99.5%) were purchased from Aldrich. All chemicals were used without further purification.

Synthesis of 5.6–10.9 nm chalcopyrite-type $CuGaS_2$ nanocrystals

Chalcopyrite $CuGaS_2$ nanocrystals were synthesized by the following procedure. Copper(I) chloride (CuCl, 0.5 mmol) and gallium chloride ($GaCl_3$, 0.5 mmol) added to OLA (10 mL) was heated to 240 °C with argon bubbling. The reaction was initiated by the rapid injection of sulfur precursor (1.0 mmol of sulfur powder dissolved into 2 mL of OLA) into the hot solution. After 1 h, the resulting solution was cooled to room temperature and treated with ethanol to precipitate orange flocculates that were subsequently separated by centrifugation. The post-treatment is essential for further narrowing the size distribution of the $CuGaS_2$ nanocrystals. Anhydrous ethanol was added dropwise to the $CuGaS_2$ nanocrystal solution until opalescence persisted upon shaking or sonication. Separation of the supernatant by centrifugation produced a precipitate enriched with the largest crystallites in the sample. The same procedures were repeated several times for subsequent supernatants containing smaller nanoparticles until a clear solution was noted. Each precipitate can disperse in non-polar organic solvents, including hexane, toluene and chloroform.

Synthesis of 3 nm chalcopyrite $CuGaS_2$ nanocrystals

In a typical synthesis of 3 nm $CuGaS_2$ nanoparticles, gallium chloride (0.5 mmol) is mixed with copper(I) chloride (0.5 mmol) and DDT (4 mL) in a three-necked flask containing OLA (6 mL). The mixture was purged with argon for 30 min. The flask was heated to 130 °C for 30 min until a transparent yellow solution formed. The temperature was then raised to 180 °C. Sulfur powder (1 mmol) dissolved in 2 mL of the OLA was rapidly injected into the reaction flask, then the color of the solution progressively changed from transparent yellow to claret-red, indicating nucleation and subsequent growth of the $CuGaS_2$ nanocrystals. After 10 min of heating, the reaction mixture was cooled to room temperature using a water bath. The crude solution was mixed with an equal volume of hexane and excess ethanol to allow flocculates to form. The nanoparticles were isolated by centrifugation at 8000 rpm for 10 min. The precipitated nanoparticles can be redispersed in toluene and washed twice with the same way to discard any remaining capping agents. The nanocrystals were then redispersed in 10 mL of hexane and centrifuged at 7000 rpm for 5 min to remove poorly capped nanocrystals and large particulates, which settled out during centrifugation. The well-capped nanocrystals can be dispersed in hexane or other organic solvents.

Synthesis of wurtzite-type $CuGaS_2$ nanocrystals and nanowires

In a typical synthesis of wurtzite $CuGaS_2$ nanocrystals, 0.5 mmol of CuCl, 0.5 mmol of $GaCl_3$, 1 mmol of thiourea and 24 mL of OLA were added to a 50 mL three-necked flask with stopcock valves in a nitrogen-filled glovebox. The stopcock valve was closed before removing the flask from the glovebox. It was connected to a Schlenk line and placed on a heating mantle. Then, the reaction mixture was heated to 240 °C under vigorous magnetic stirring. After 1 h, the crude solution was cooled to room temperature using a water bath and then centrifuged at 7000 rpm for 5 min with 10 mL hexane to remove large clusters. The supernatant of nanoparticles can be separated by further centrifugation at 8000 rpm for 10 min with 10 mL hexane and 15 mL ethanol.

Wurtzite $CuGaS_2$ nanowires were synthesized with the same procedure but using 12 mL of OLA instead of 24 mL. The crude solution was centrifuged at 8000 rpm for 10 min with 10 mL hexane and 15 mL ethanol to remove unreacted precursors. The purified nanoparticles and nanowires were redispersed in toluene for further characterization without any size sorting.

Characterization

The morphologies of the as-grown $CuGaS_2$ nanocrystals were analysed by transmission electron microscopy (TEM) and high resolution TEM (HRTEM). A Topcon EM002B electron microscope operating at 200 kV was used for the TEM. Samples were prepared by placing a drop of a dilute dispersion of nanocrystal solution on the surface of a copper grid (300 mesh) coated with an amorphous carbon film. The crystal structures were determined using X-ray powder diffraction (XRD) on a Rigaku 300 Rotaflex diffractometer operating in the Bragg configuration using Cu Kα radiation. The accelerating voltage was set at 250 kV with a 200 mA flux. Scatter and diffraction slits of

0.50° and a 0.15 mm collection slit were used. For elemental analysis, a Tecnai F30ST (FEI) instrument with a field emission gun was equipped with an Energy-Dispersive Spectroscopy (EDS) spectrometer for EDS analysis. UV-Vis spectra were recorded using a Hitachi U-4100 UV-Vis-NIR spectrophotometer at room temperature. PL spectra were taken using a Spex Fluorolog-3 fluorometer.

3. Results and discussion

3.1 Synthesis of chalcopyrite $CuGaS_2$ nanocrystals

For ternary I–III–VI_2 nanocrystal synthesis, how to balance the reaction activity of each reagent needs to be greatly considered to avoid the formation of heterostructures, as core/shell, composite structure, or even two compounds. Metal chlorides dissolved in OLA as reactants were used to prepare chalcopyrite-type $CuInS_2$, $CuInSe_2$, $CuIn(S_xSe_{1-x})_2$ and $Cu(In_{1-x}Ga_x)(S_ySe_{1-y})_2$ nanoparticles.[21,22] OLA serves as a good surfactant for forming metal chalcogenide nanocrystals and could reduce the reactivity difference between the Cu, In, Ga, Se and S reactants. Chalcopyrite-type $CuGaS_2$ nanocrystals were synthesized through a thermal decomposition method. $GaCl_3$ dissolved in OLA could be directly used as a Ga source. Sulfur powder dissolved in OLA with a short duration of sonication was injected into the preheated metal halides/OLA solution and kept at 240 °C for 1 h, by adding CuCl, $GaCl_3$ and S powder as Cu, Ga and S source to the reaction:

$$CuCl + GaCl_3 + S \xrightarrow{\text{OLA, 240 °C}} CuGaS_2 \text{ nanocrystals} + \text{byproducts} \quad (1)$$

Fig. 1a shows the XRD pattern of the product, in which only chalcopyrite $CuGaS_2$ peaks are observed without any impurity peak. In the previous synthesis of $CuInS_2$ nanocrystals, the difference between the chalcopyrite phase and zinc blende phase is very small, but the $CuInS_2$ nanocrystals with the zinc blende phase usually have a diffraction peak of (200).[41–43] In our work, the absence of this peak in the XRD patterns of $CuGaS_2$ nanocrystals can be considered as evidence for the chalcopyrite phase. The TEM image of the $CuGaS_2$ nanocrystals (Fig. 1b) shows that the nanocrystals are spherical in shape, but with a relatively broad size distribution. HRTEM (Fig. 1c) of one nanocrystal shows its high crystallinity nature; the lattice fringes of the $CuGaS_2$ nanoparticles show a spacing of d = 0.19 nm and d = 0.31 nm, which corresponds to the (220) and (112) lattice planes of the chalcopyrite of $CuGaS_2$. The FFT image of the HRTEM image along the zone axis of the [−110] direction is also consistent with chalcopyrite $CuGaS_2$. The corresponding $CuGaS_2$ crystal structure is shown in Fig. 1d.

In order to obtain nanoparticles with more uniform sizes, a precipitation procedure was applied to narrow down the size distribution. Ethanol, serving as a polar anti-solvent, was introduced to the concentrated $CuGaS_2$ solution dropwise until the $CuGaS_2$ nanocrystals started to precipitate, resulting in opalescence and a turbid solution. The reason for this phenomenon is that the decrease of the ligand–solvent interaction causes particles to become unstable in solution. Further, the different sizes of the $CuGaS_2$ nanoparticles can be separated by centrifugation. With several cycles of the isolation procedure, different sizes of $CuGaS_2$ nanoparticles can be obtained. Fig. 2 shows the TEM images of $CuGaS_2$

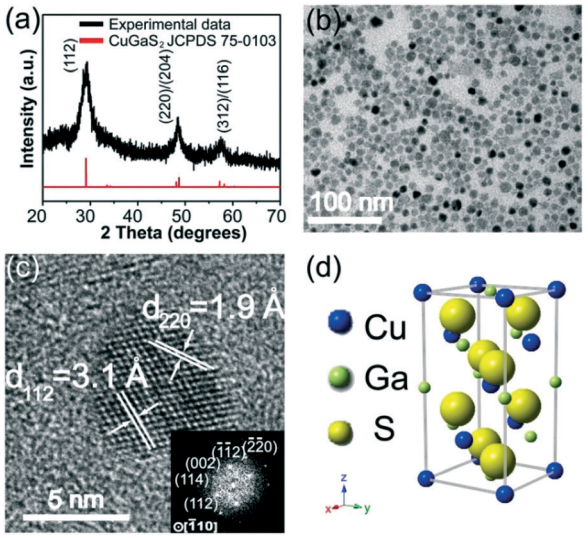

Fig. 1 Chalcopyrite $CuGaS_2$ nanocrystals synthesized from CuCl, $GaCl_3$, and S with OLA as surfactant at 240 °C for 1 h. (a) XRD, (b) TEM, (c) HRTEM and corresponding FFT image and (d) simulated unit cell of chalcopyrite $CuGaS_2$.

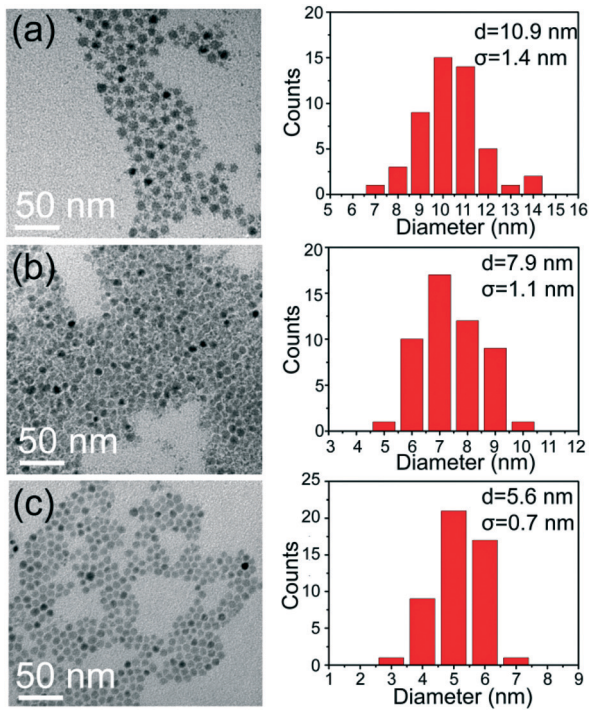

Fig. 2 TEM image and size distribution histogram of chalcopyrite $CuGaS_2$ nanoparticles with an average size of (a) 10.9 ± 1.4 nm (b) 7.9 ± 1.1 nm (c) 5.6 ± 0.7 nm.

nanoparticles at each size-selective precipitation step and the $CuGaS_2$ nanocrystals with nearly monodisperse nanocrystals were obtained. The average diameters of the three samples are 10.9 ± 1.4 nm, 7.9 ± 1.1 nm, and 5.6 ± 0.7 nm, respectively.

On the other hand, we find that using a combination of DDT and OLA in the reaction can allow us to obtain smaller $CuGaS_2$ nanocrystals. It was noticed that thiols can serve as the stabilizing ligand and the solvent in the reaction. Thiols can also play the role of the sulfur source, which forms thiolates with metal ions.[44] Fig. 3a shows the XRD pattern of a $CuGaS_2$ nanocrystal prepared using 8 mL OLA and 4 mL DDT. The diameter of the nanocrystals is approximately 3.0 ± 0.4 nm. Both XRD and HRTEM confirmed that the nanocrystals are crystalline with a chalcopyrite $CuGaS_2$ structure. The *d*-spacing observed in the HRTEM image is also consistent with chalcopyrite $CuGaS_2$.

Fig. 4a shows the UV-Vis absorbance spectra of the four samples of different sizes of chalcopyrite $CuGaS_2$ nanoparticles dispersed in toluene. The absorption edge shows the blue-shift upon decreasing the size of the nanocrystals, exhibiting quantum-dot-like behavior. The nature of the broad emission peak was completely observed (Fig. 4b), and the PL spectra match well with absorption spectra for the samples after the size sorting. It also shows a blue-shift while the size decreased in the PL spectra. In Fig. 4c, the experimental values are consistent with theoretical calculation in the size range below 6 nm.[45]

3.2 Synthesis of wurtzite $CuGaS_2$ nanocrystals

Wurtzite $CuGaS_2$ nanoparticles can be synthesized using thiourea as a sulfur source with OLA. The XRD pattern (Fig. 5a) shows the characteristic of hexagonal cell with the space group of *P*63*mc*. The cell parameters and corresponding structural parameters are shown in Table 1.

The as-synthesized wurtzite $CuGaS_2$ nanocrystals are polydisperse with a mean diameter of 29.9 ± 6.6 nm, as determined

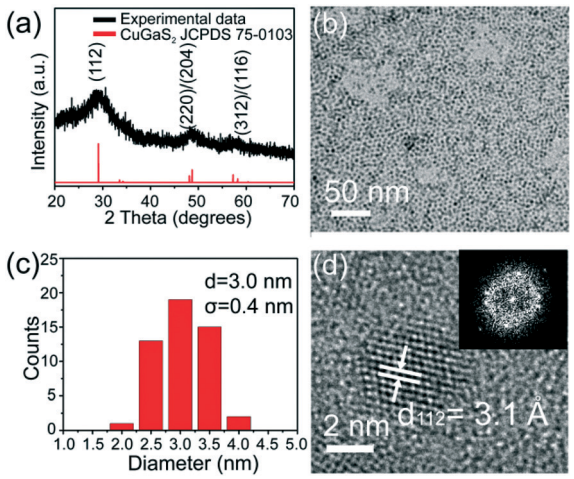

Fig. 3 OLA and DDT capped $CuGaS_2$ chalcopyrite nanocrystals synthesized at 180 °C for 10 min. The nanoparticles with the average size of 3.0 ± 0.4 nm were obtained. (a) XRD pattern, (b) the TEM image, (c) size distribution histogram and (d) HRTEM image.

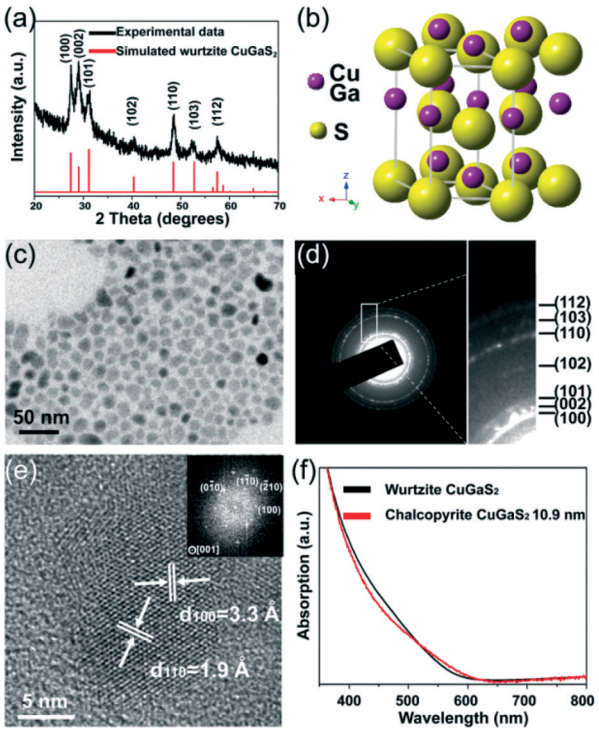

Fig. 5 Wurtzite $CuGaS_2$ nanocrystals synthesized from CuCl, $GaCl_3$ and thiourea with 24 mL OLA as surfactant at 240 °C for 1 h. (a) XRD, (b) crystal structure of wurtzite crystal structure. Note that Cu and Ga atoms occupy the same position. (c, d) TEM and corresponding SAED, (e) HRTEM and corresponding FFT, and (f) UV-Vis spectra (comparison to chalcopyrite $CuGaS_2$) of wurtzite $CuGaS_2$ nanocrystals.

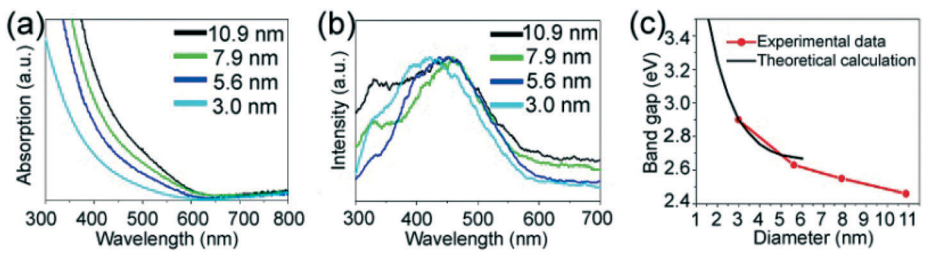

Fig. 4 (a) UV-Vis absorbance spectra and (b) corresponding PL of different sizes of chalcopyrite $CuGaS_2$ nanocrystals. (c) The comparison of optical band gap with theoretical band gap.[45]

Table 1 Crystal parameters of wurtzite $CuGaS_2$

Atom	Wyck.	x/a	y/b	z/c
Cu	2b	1/3	2/3	0
Ga	2b	1/3	2/3	0
S	2b	1/3	2/3	0.3752

by TEM analysis (Fig. 5c). Also, no other crystal phases were observed by SAED analysis (Fig. 5d). The HRTEM image shows an apparent single crystalline particle with the (100) and (110) lattice planes, displaying a *d*-spacing of 0.33 nm and 0.19 nm as shown in Fig. 5e. The optical spectrum of the wurtzite $CuGaS_2$ nanocrystals is similar to the optical absorption spectra of chalcopyrite $CuGaS_2$ nanoparticles (Fig. 5f). The band gap of the wurtzite $CuGaS_2$ nanocrystals was determined from the onset of the UV-Vis absorption spectrum to be E_g = 2.47 eV, while bulk chalcopyrite $CuGaS_2$ has a reported band gap between 2.4 and 2.5 eV. EDS analysis (ESI,† Fig. S3) indicates that the chemical composition of the product is composed of Cu, Ga and S with a molar ratio of 1 : 1 : 1.96, which is close to the stoichiometric composition of $CuGaS_2$.

Decreasing the amount of OLA favours the formation of nanowires. When the amount of OLA decreased from 24 mL to 12 mL, $CuGaS_2$ nanowires were produced as shown in Fig. 6. All solid nanowires were found to be highly-crystalline with the wurtzite crystal structure. The average length of the nanowires is typically over 4 μm, while the average diameter can be formed in the range between 50 and 100 nm. The HRTEM images (Fig. 6e and 6f) and their corresponding SAED patterns (insets of Fig. 6e and 6f) are analyzed. Two nanowire sections with the same FFT are shown. The FFTs can be indexed alone the [001] zone axis and two directions along [110] and [100] can be observed. These data suggest that the curvature of the $CuGaS_2$ nanowires was formed by oriented attachment.

When an equal volume of DDA was substituted for OLA under otherwise identical conditions, the wurtzite phase of the $CuGaS_2$ nanocrystals and nanorods ($W < 100$ nm, $L < 200$ nm) was produced without the formation of any nanowires (Fig. 7). This suggests that the presence of different chains of the primary amine has an influence on the product morphology.

In addition, further experiments indicate that the reactant concentration strongly influences the nanowire formation. When the concentration of reactants was decreased to one-fifth of the typical nanowire growth solution, no nanowires were found. Fig. 8a exhibits the typical morphology of a short wire and its magnified image is shown in Fig. 8b. Further observation reveals that the structure of the short wires comprises several small wurtzite $CuGaS_2$ nanoparticles.

The growth mechanism of nanowires. To better understand the growth mechanism of the wurtzite $CuGaS_2$ nanowires, products collected at different reaction temperatures in OLA were characterized by TEM and XRD as shown in Fig. 9. The nucleation and growth of nanowires were highly dependent on the reaction temperature. In the first step, small $CuGaS_2$ nuclei were formed at 130 °C (Fig. 9a). Even though the reaction time

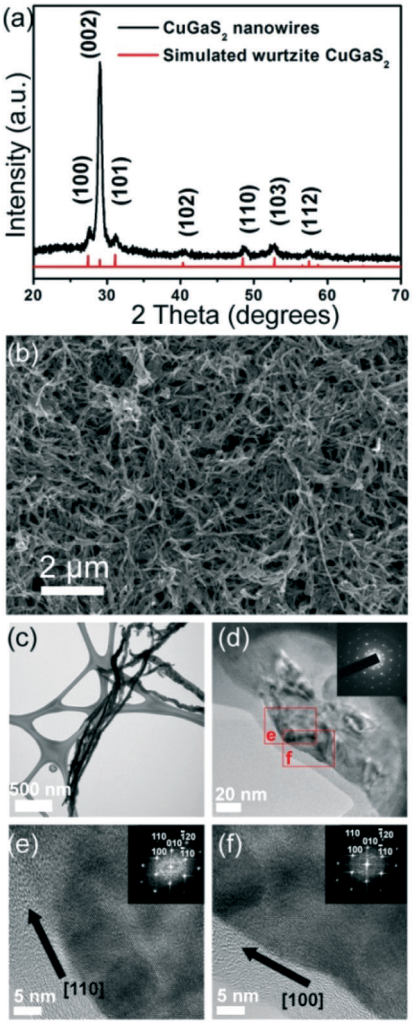

Fig. 6 Wurtzite $CuGaS_2$ nanowires synthesized from CuCl, $GaCl_3$ and thiourea with 12 mL OLA as surfactant at 240 °C for 1 h. (a) XRD pattern, and (b) SEM image, (c, d) TEM image, and (e, f) HRTEM of wurtzite $CuGaS_2$ nanowires.

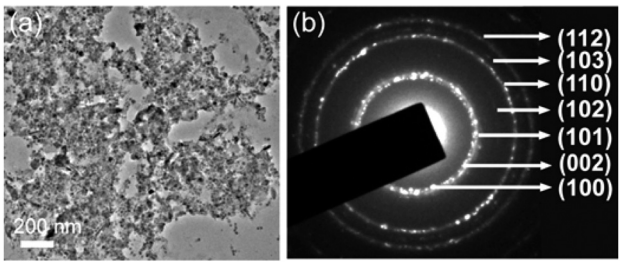

Fig. 7 Wurtzite $CuGaS_2$ nanocrystals synthesized from CuCl, $GaCl_3$ and thiourea with 12 mL DDA as surfactant at 240 °C for 1 h. (a) TEM image and (b) corresponding SAED pattern of wurtzite $CuGaS_2$ nanoparticles capped by DDA.

was prolonged to 1 h, no wire-like nanocrystals can be found in the product. $CuGaS_2$ nanoparticles aggregated together when temperature was raised to 180 °C (Fig. 9b). Nanowires were formed by increasing the reaction temperature to 200 °C.

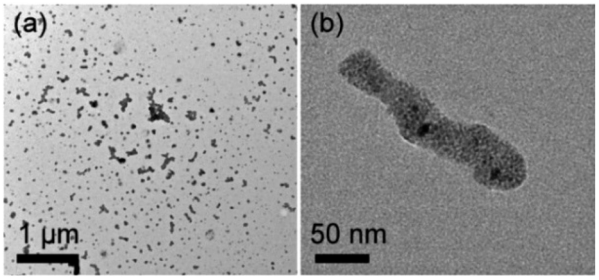

Fig. 8 TEM image of wurtzite $CuGaS_2$ nanorods synthesized from 0.1 mmol CuCl, 0.1 mmol $GaCl_3$ and 0.2 mmol thiourea (1/5 of the typical reactant concentration) with 12 mL OLA as surfactant at 240 °C for 1 h.

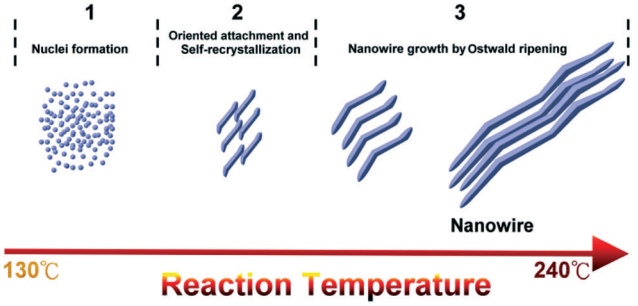

Scheme 1 Schematic illustration of the growth mechanism of the obtained wurtzite $CuGaS_2$ nanowires.

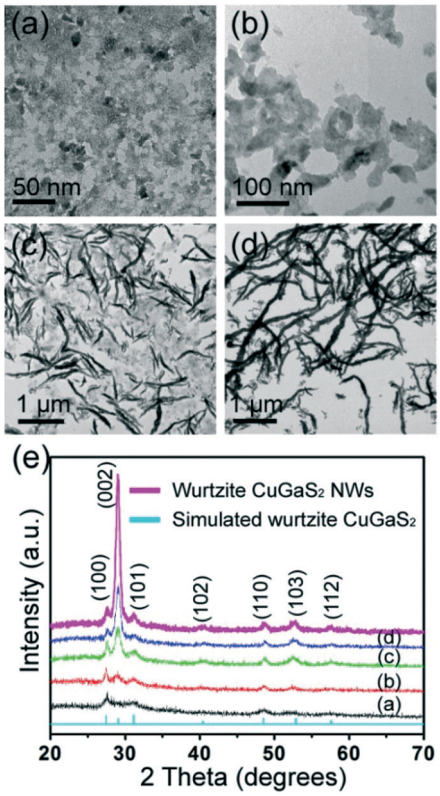

Fig. 9 TEM image of wurtzite $CuGaS_2$ nanocrystals synthesized from CuCl, $GaCl_3$ and thiourea with 12 mL OLA as surfactant at (a) 130 °C (b) 180 °C (c) 200 °C (d) 240 °C for 5 min, (e) and their corresponding XRD patterns.

Rearrangement of the short $CuGaS_2$ nanowires in the length range of 100 nm to 1 μm was observed (Fig. 9c). The growth of $CuGaS_2$ nanocrystals could be due to oriented attachment and Ostwald ripening.[46] In Fig. 9d, further growth of the $CuGaS_2$ nanowires took place while the reaction temperature was increased to 240 °C. The nanowires collected at 240 °C for 5 min have lengths ranging from 100 nm to 4 μm. XRD characterization (Fig. 9e) was conducted at the various growth stages and reveals that all products are the wurtzite structure of $CuGaS_2$. Interestingly, the (002) reflection observed in the XRD patterns becomes stronger with increasing reaction temperature, but other peak reflections increase more slowly without changing the position of the peaks. The result suggests that the $CuGaS_2$ nanowires are preferentially oriented and the (002) peak. The relationship between the reaction temperature and the morphology evolution of $CuGaS_2$ nanowires is summarized as a schematic diagram (Scheme 1).

4. Conclusions

In summary, we have developed a systematic synthetic approach to obtain different sizes, phases, shapes of $CuGaS_2$ nanocrystals (Table 2). Different sizes of chalcopyrite $CuGaS_2$ nanoparticles exhibit the size-dependent optical properties consistent with theoretical calculation. The sulfur source plays a pivotal role in the crystal phase determination: sulfur powder leads to chalcopyrite $CuGaS_2$ and thiourea leads to the wurtzite phase. In the synthesis of wurtzite $CuGaS_2$, a smaller amount of OLA promotes anisotropic growth. It was observed that the formation of these nanowires through oriented attachment accompanied with Ostwald ripening by observing the morphology evolution of the products from 130 to 240 °C. These results show a different synthetic path to obtaining I–III–VI group nanowires compared with existing examples for ternary nanowires grown by the vapor–liquid–solid method (VLS), solution–liquid–solid method (SLS) and phase transformation mechanisms.

Table 2 Experimental parameters and their results

Fig. no.	Sulfur source	Stabilizing agents, solvent	Reaction temp. (°C)	Crystalline phase	Morphology
Fig. 2	Sulfur	OLA (12 mL)	240	Chalcopyrite	Nanoparticles (5–11 nm)
Fig. 3	Sulfur	OLA (8 mL), DDT (4 mL)	180	Chalcopyrite	Nanoparticles (3 nm)
Fig. 5	Thiourea	OLA (24 mL)	240	Wurtzite	Nanoparticles (29.9 ± 6.6 nm)
Fig. 6	Thiourea	OLA (12 mL)	240	Wurtzite	Nanowires
Fig. 7	Thiourea	DDA (12 mL)	240	Wurtzite	Aggregated nanoparticles (5–8 nm)

Acknowledgements

We acknowledge the financial support from the National Science Council of Taiwan (NSC 102-2221-E-007-023-MY3, NSC 102-2221-E-007-090-MY2, NSC 101-2623-E-007-013-IT, and NSC102-2633-M-007-002), the Ministry of Economic Affairs, Taiwan (101-EC-17-A-09-S1-198), National Tsing Hua University (102N2051E1 and 102N2061E1), and the assistance from Center for Energy and Environmental Research, National Tsing-Hua University.

References

1 J. Xu, C. S. Lee, Y. B. Tang, X. Chen, Z. H. Chen, W. J. Zhang, S. T. Lee, W. X. Zhang and Z. H. Yang, *ACS Nano*, 2010, **4**, 1845–1850.
2 W. E. Devaney, W. S. Chen, J. M. Stewart and R. A. Mickelsen, *IEEE Trans. Electron Devices*, 1990, **37**, 428–433.
3 R. Scheer, T. Walter, H. W. Schock, M. L. Fearheiley and H. J. Lewerenz, *Appl. Phys. Lett.*, 1993, **63**, 3294–3296.
4 V. A. Akhavan, B. W. Goodfellow, M. G. Panthani, D. K. Reid, D. J. Hellebusch, T. Adachi and B. A. Korgel, *Energy Environ. Sci.*, 2010, **3**, 1600–1606.
5 H. Ye, H. S. Park, V. A. Akhavan, B. W. Goodfellow, M. G. Panthani, B. A. Korgel and A. J. Bard, *J. Phys. Chem. C*, 2010, **115**, 234–240.
6 Q. Guo, S. J. Kim, M. Kar, W. N. Shafarman, R. W. Birkmire, E. A. Stach, R. Agrawal and H. W. Hillhouse, *Nano Lett.*, 2008, **8**, 2982–2987.
7 Q. Guo, G. M. Ford, H. W. Hillhouse and R. Agrawal, *Nano Lett.*, 2009, **9**, 3060–3065.
8 W. Liu, D. B. Mitzi, M. Yuan, A. J. Kellock, S. J. Chey and O. Gunawan, *Chem. Mater.*, 2009, **22**, 1010–1014.
9 M.-Z. Xue and Z.-W. Fu, *Thin Solid Films*, 2008, **516**, 8386–8392.
10 W. Zhang, H. Zeng, Z. Yang and Q. Wang, *J. Solid State Chem.*, 2012, **186**, 58–63.
11 M. G. Panthani, T. A. Khan, D. K. Reid, D. J. Hellebusch, M. R. Rasch, J. A. Maynard and B. A. Korgel, *Nano Lett.*, 2013, **13**, 4294–4298.
12 C. J. Hibberd, E. Chassaing, W. Liu, D. B. Mitzi, D. Lincot and A. N. Tiwari, *Prog. Photovoltaics*, 2010, **18**, 434–452.
13 Y. G. Cai, J. C. W. Ho, S. K. Batabyal, W. Liu, Y. Sun, S. G. Mhaisalkar and L. H. Wong, *ACS Appl. Mater. Interfaces*, 2013, **5**, 1533–1537.
14 M. G. Panthani, V. Akhavan, B. Goodfellow, J. P. Schmidtke, L. Dunn, A. Dodabalapur, P. F. Barbara and B. A. Korgel, *J. Am. Chem. Soc.*, 2008, **130**, 16770–16777.
15 V. A. Akhavan, B. W. Goodfellow, M. G. Panthani, C. Steinhagen, T. B. Harvey, C. J. Stolle and B. A. Korgel, *J. Solid State Chem.*, 2012, **189**, 2–12.
16 S.-H. Chang, M.-D. Lu, Y.-L. Tung and H.-Y. Tuan, *ACS Nano*, 2013, **7**, 9443–9451.
17 Y.-G. Chun, K.-H. Kim and K.-H. Yoon, *Thin Solid Films*, 2005, **480**, 46–49.
18 W.-C. Huang, C.-H. Tseng, S.-H. Chang, H.-Y. Tuan, C.-C. Chiang, L.-M. Lyu and M. H. Huang, *Langmuir*, 2012, **28**, 8496–8501.
19 W. H. Hsu, H. I. Hsiang, Y. L. Chang, D. T. Ray and F. S. Yen, *J. Am. Ceram. Soc.*, 2011, **94**, 3030–3034.
20 B. Koo, R. N. Patel and B. A. Korgel, *Chem. Mater.*, 2009, **21**, 1962–1966.
21 M.-Y. Chiang, S.-H. Chang, C.-Y. Chen, F.-W. Yuan and H.-Y. Tuan, *J. Phys. Chem. C*, 2011, **115**, 1592–1599.
22 S.-H. Chang, M.-Y. Chiang, C.-C. Chiang, F.-W. Yuan, C.-Y. Chen, B.-C. Chiu, T.-L. Kao, C.-H. Lai and H.-Y. Tuan, *Energy Environ. Sci.*, 2011, **4**, 4929–4932.
23 Q. Li, L. Zhai, C. Zou, X. Huang, L. Zhang, Y. Yang, X. A. Chen and S. Huang, *Nanoscale*, 2013, **5**, 1638–1648.
24 A. J. Wooten, D. J. Werder, D. J. Williams, J. L. Casson and J. A. Hollingsworth, *J. Am. Chem. Soc.*, 2009, **131**, 16177–16188.
25 M. Kruszynska, H. Borchert, A. Bachmatiuk, M. H. Rümmeli, B. Büchner, J. R. Parisi and J. Kolny-Olesiak, *ACS Nano*, 2012, **6**, 5889–5896.
26 O. Yarema, D. Bozyigit, I. Rousseau, L. Nowack, M. Yarema, W. Heiss and V. Wood, *Chem. Mater.*, 2013, **25**, 3753–3757.
27 J. Hu, L.-S. Li, W. Yang, L. Manna, L.-W. Wang and A. P. Alivisatos, *Science*, 2001, **292**, 2060–2063.
28 Y. N. Xia, P. D. Yang, Y. G. Sun, Y. Y. Wu, B. Mayers, B. Gates, Y. D. Yin, F. Kim and Y. Q. Yan, *Adv. Mater.*, 2003, **15**, 353–389.
29 Z. Tang and N. A. Kotov, *Adv. Mater.*, 2005, **17**, 951–962.
30 M. Giersig, I. Pastoriza-Santos and L. M. Liz-Marzan, *J. Mater. Chem.*, 2004, **14**, 607–610.
31 K.-S. Cho, D. V. Talapin, W. Gaschler and C. B. Murray, *J. Am. Chem. Soc.*, 2005, **127**, 7140–7147.
32 C. Pacholski, A. Kornowski and H. Weller, *Angew. Chem., Int. Ed.*, 2002, **41**, 1188–1191.
33 X. Lu, Z. Zhuang, Q. Peng and Y. Li, *CrystEngComm*, 2011, **13**, 4039–4045.
34 F. Wang, Y. Han, C. S. Lim, Y. H. Lu, J. Wang, J. Xu, H. Y. Chen, C. Zhang, M. H. Hong and X. G. Liu, *Nature*, 2010, **463**, 1061–1065.
35 Y. H. A. Wang, X. Y. Zhang, N. Z. Bao, B. P. Lin and A. Gupta, *J. Am. Chem. Soc.*, 2011, **133**, 11072–11075.
36 S. Levcenko, N. Syrbu, V. Tezlevan, E. Arushanov, S. Doka-Yamigno, T. Schedel-Niedrig and M. C. Lux-Steiner, *J. Phys.: Condens. Matter*, 2007, **19**, 456222.
37 M. D. Regulacio, C. Ye, S. H. Lim, Y. Zheng, Q. Xu and M. Han, *CrystEngComm*, 2013, **15**, 5214–5217.
38 J. Hu, B. Deng, C. Wang, K. Tang and Y. Qian, *Solid State Commun.*, 2002, **121**, 493–496.
39 Q. Lu, J. Hu, K. Tang, Y. Qian, G. Zhou and X. Liu, *Inorg. Chem.*, 2000, **39**, 1606–1607.
40 Q. Li, C. Zou, L. Zhai, J. Shen, L. Zhang, H. Yu, Y. Yang, X. A. Chen and S. Huang, *J. Alloys Compd.*, 2013, **567**, 127–133.
41 K. Nose, Y. Soma, T. Omata and S. Otsuka-Yao-Matsuo, *Chem. Mater.*, 2009, **21**, 2607–2613.
42 D. C. Pan, L. J. An, Z. M. Sun, W. Hou, Y. Yang, Z. Z. Yang and Y. F. Lu, *J. Am. Chem. Soc.*, 2008, **130**, 5620–5621.

43 G. D. Scholes, H. Z. Zhong, S. S. Lo, T. Mirkovic, Y. C. Li, Y. Q. Ding and Y. F. Li, *ACS Nano*, 2010, **4**, 5253–5262.
44 D. Aldakov, A. Lefrançois and P. Reiss, *J. Mater. Chem. C*, 2013, **1**, 3756–3776.
45 T. Omata, K. Nose and S. Otsuka-Yao-Matsuo, *J. Appl. Phys.*, 2009, **105**, 073106.
46 H. Zhong, Y. Zhou, M. Ye, Y. He, J. Ye, C. He, C. Yang and Y. Li, *Chem. Mater.*, 2008, **20**, 6434–6443.

